2022-01-0495 Published 29 Mar 2022

High-Speed Thermographic Analysis of Diesel Injector Nozzle Tip Temperature

Alex Gander University of Brighton

Cyril Crua and Dan Sykes University of Brighton

Rob Spragg bp

Guillaume de Sercey University of Brighton

Raul Payri Universitat Politecnica de Valencia

Cameron Webb bp

Citation: Gander, A., Crua, C., Sykes, D., Spragg, R. et al., "High-Speed Thermographic Analysis of Diesel Injector Nozzle Tip Temperature," *SAE Int. J. Advances & Curr. Prac. in Mobility* 4(5):1734-1741, 2022, doi:10.4271/2022-01-0495.

This article was presented at the WCX World Congress Experience, April 5-7, 2022.

Received: 05 Nov 2021 Revised: 24 Dec 2021 Accepted: 12 Jan 2022

Abstract

The temperature of fuel injectors can affect the flow inside nozzles and the subsequent spray and liquid films on the injector tips. These processes are known to impact fuel mixing, combustion and the formation of deposits that can cause engines to go off calibration. However, there is a lack of experimental data for the transient evolution of nozzle temperature throughout engine cycles and the effect of operating conditions on injector tip temperature. Although some measurements of engine surface temperature exist, they have relatively low temporal resolutions and cannot be applied to production injectors due to the requirement for a specialist coating which can interfere with the orifice geometry. To address this knowledge gap, we have developed a high-speed infrared imaging approach to measure the temperature of the nozzle surface inside an optical diesel engine. We investigated ways of increasing the emissivity of the nozzle surface with minimal intrusion by applying thin carbon coatings. We compare our measurements with those from a production injector that was instrumented with internal thermocouples. Our steady-state off-engine investigation showed that nozzle surface temperature measured by infrared imaging could yield data at 1200 fps with uncertainties of +20K to -1K compared to simultaneous thermocouple measurements. We applied this approach to an optical diesel engine to investigate the effect of injection duration and increased swirl ratio on injector nozzle temperature and surface homogeneity.

Introduction

Recent changes in road vehicle emissions regulations have placed increased pressure on automotive engineers to develop and progress vehicle technology in order to meet the targets set out by the legislators. A well-known issue central to vehicle emissions is the poor combustion quality. This is due to insufficient mixing of the fuel and air, which can lead to increases in pre-catalyst engine emissions [1]. Therefore, to achieve a decrease in emissions output of an internal combustion engine, there is a requirement to improve the accuracy between the approximated and real fuel injection temperatures as these variables are fundamental for any combustion study [2]. The temperature of the fuel is known to affect liquid and vapour penetration lengths, as well as ignition delay, which contributes to pre-catalyst engine-out emissions [3]. Higher fuel temperatures have been seen to increase CO_2, un-burnt hydrocarbon emissions and increased brake thermal efficiency while decreasing NO_X [4, 5]. It has been suggested that fuel temperature is very closely related to the temperature of the fuel injector [6], hence if a temperature measurement of the fuel injector is made, it may be possible to infer the fuel's temperature during the injection.

Fuel and injector nozzle temperatures also have a significant impact on the near nozzle fluid dynamics throughout and after the injection process [7]. The fluid dynamic processes post-injection for diesel injectors are now well defined into several phases. These stages contribute to fuel film formation and subsequent, carbon deposits formation [8, 9]. The quantity of fuel deposited on the nozzle surface is also highly dependant on the fuel temperature due to the significant effect that temperature has on surface tension, and viscosity [10]. The limited amount of available crank angle resolved data has

impeded progress in evaluating thoroughly the dynamics of bubbling and evaporation phenomena of fuel films late in the engine cycle, which are affected by the in-cylinder gas and surface temperatures [11, 9]. Many methods have been explored to evaluate the injector nozzle and fuel temperature, although all have limitations, including the thermography approach discussed here. The key challenge facing these methods is the high temporal resolution required to capture the highly transient thermal evolution of in-engine surfaces across the cycle, compounded with the hostile environment found inside a combustion chamber and the difficulty accessing the internal surfaces either physically or optically. One such method used to overcome this is to modify a fuel injector nozzle to allow a thermocouple to be fitted beneath the injector surface, as close to the injector tip as possible without compromising the internal injector geometry [11, 12]. However, embedding thermocouples inside injector tips remains a complex and risky approach due to the machining process weakening the nozzle tips, potentially leading to a mechanical failure of the injector nozzle and catastrophic engine damage. Members of the Engine Combustion Network found that nozzle temperature measurements in spray vessels and engines resulted in significant differences, possibly due to different locations and contact of the thermocouples on the surfaces. Additionally, the slow time constants of thermocouples limits readings to measurement frequencies in the order of 1 Hz. [13, 14]. An alternative method known as laser-induced phosphorescence uses the luminescent properties of thermographic phosphors to infer the surface's temperature. To utilise the phosphor's properties, it is excited with a coherent light source with the intensity of the light emitted from the phosphor recorded. After that, the decay time of the light emitted is a function of temperature [13]. Laser-induced phosphorescence can provide crank angle-resolved measurements. However, due to the emission signal of the phosphor being very low, it can encounter issues during the combustion process with the phosphor signal getting masked by the natural combustion luminosity [15]. Moreover, in the investigations conducted by Kashdan et al. [15] the amplified photodetector used only allowed for the measurement of a 1 mm disc, which is insufficient to properly characterise the thermal evolution of the injector nozzle tip across an engine cycle. Due to the lack of available experimental data, the thermal profile of the injector nozzle is often approximated via a numerical methodology [6].

Because of the lack of available data and approximations currently being used to evaluate the thermal evolution of the injector nozzle surface, the motivation for this study is to demonstrate the high-speed infrared thermography approach as a method to characterise further the thermal transients found in internal combustion engines. Thermographic measurements were made using a high-speed infrared camera operating in the mid-wave infrared range in conjunction with a Bowditch style optical 4-stroke diesel engine. The measurements were conducted using a production multi-hole valve-covered orifice (VCO) diesel injector using multi-component (CEC-RF79) fuel. Post-calibration, our infrared approach showed advantages over previously discussed techniques due to its spatial and temporal resolutions and the non-intrusive nature of the approach. This article is structured into three main components, including the introduction. The second section discusses the experimental setup and calibration methodologies, and the third section presents the results from the study evaluating the effect of injection duration and swirl ratio on injector nozzle tip temperature. Finally, a summary of the key finding can be found in the conclusion.

Experimental Setup

Optical Engine Configuration

Experiments were undertaken using a 4-stroke Bowditch style optical diesel engine based on a production PUMA engine with 86 mm bore and stroke and fitted with a Delphi DFI 1.3 VCO direct injection (DI) diesel injector. To emulate low-load and idle conditions, the engine is supplied boost pressure from an external pressure reservoir filled by a compressor that feeds the engine a constant intake flow rate using a set of critical flow venturi nozzles. For further adaptability, the engine testbed is equipped with a swirl valve on the intake manifold. This allows the swirl to be varied between a ratio of 1.38 and 4.12, where the ratio is equal to the average rotational velocity of the free charge vortex, divided by the charge vortex as a rigid body rotating on its axis [16, 17]. The engine runs a 1:64 skip fire regime to reduce fouling of the optical surfaces. However, due to the engine not being fired continuously, the coolant used to heat the engine testbed to ≈55 °C and allows a stable temperature to be maintained whilst still emulating idle to light load conditions. The crank was spun at 1000 rpm using a 30 kW dynamometer with several engine operating conditions swept during the investigations. Figure 1 shows the engine testbed and optical configurations.

The testbed is also instrumented with temperature and pressure sensors on all the major ancillary systems such as intake air, oil, coolant and fuel systems, crank angle position logged by an optical encoder with a resolution of 0.5° Crank

FIGURE 1 Configuration of bowditch style optical engine and Telops M100*k* infrared camera setup.

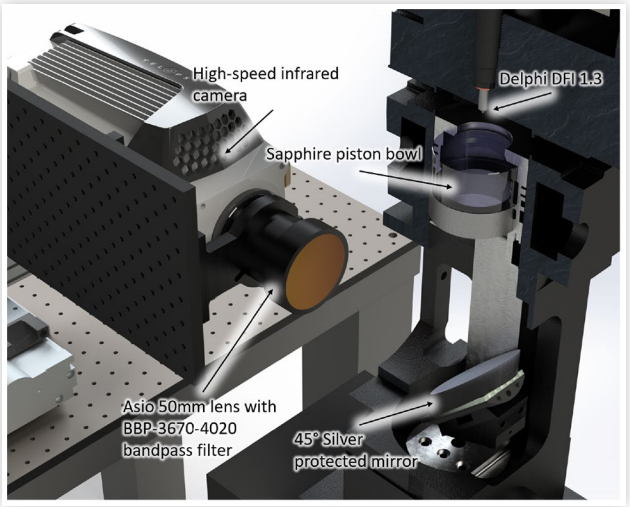

TABLE 1 Engine setup and configuration for investigations.

Parameter	Value
Engine Speed	1000 RPM
Compression Ratio	14:1
Injector	Delphi DFI 1.3
Start of injection	−18° CA aTDC
Injector pulse duration	1000 µs; 2000 µs
Fuel	CEC RF-79
Swirl ratio	1.38; 4.12
Stroke	4

TABLE 2 Camera operation parameters for investigations.

Parameter	Value
Camera	Telops Fast M100*k*
Wavelength range	3000 to 4900 nm
Frame size	80 × 80 pixels^2
Calibrated well capacity	8 Me-
NETD	14.2 mK (measured)
Infrared lens	Janos Technology Asio 50 mm, f/2.3
Infrared transmittance	>93% at 25 °C
Measured scale factor	88.75 µm/pixel

Angle (CA). A piezoelectric pressure sensor (Kistler 6125C) is implemented to take high-speed data acquisition with a sample taken every 0.5° CA. A purpose-built LabVIEW interface manages the testbed, and injection system, while also managing the low and high-speed data acquisition accurate to 1 s and 25 ns respectively. The fuel system is comprised of a light-duty lift pump (rated to 0.2 MPa), a high-pressure pump rated to 160 MPa (Bosch CP1H), a vacuum venturi line to provide the injector with the appropriate pressure on the injector leak offline and two pressure sensors, one on the common rail (Bosch 51HP02-02) and one on the injector feed (Kistler 4067E). In this investigation, the Delphi DFI 1.3 VCO injector was instrumented with a Tactical 306, Type-K thermocouple, providing time-averaged nozzle surface temperature. However, the machining process to instrument the fuel injector with the thermocouple compromises the integrity of the nozzle, therefore, limiting its safe operating pressure to 400 bar.

The optical engine is fitted with a sapphire bowl (68 mm diameter, 33 mm thickness) on an extended Bowditch style piston, allowing for a stationary silver-coated mirror to be fitted at 45° to the cylinder as shown in Figure 1. Having the mirror mounted at 45° allows the radiation emitted from the injector nozzle to be deflected and captured by the camera sensor. In order to prevent the camera's sensor from becoming over-saturated, the cameras exposure time was changed between test points from 100 µs to 400 µs depending on the expected peak temperature. The setup described in Figure 3 allows for the visualisation of the entire injector nozzle surface with a scale factor of 88.75 µm/pixel, which was sufficient to see a detailed structure of the nozzle tip. Table 1 shows the engine operating conditions and parameters used in these investigations.

High-Speed Infrared Camera Calibration

To enable crank angle resolved temperature measurements to be taken, a high-speed mid-wave infrared camera (Telops M100*k*) was used at the operating conditions listed in Table 2. A 50 mm lens was used, factory calibrated by the manufacturer for a temperature range of -50 °C up to 2500 °C. This also accounted for the pixel to pixel non-uniformity in sensor irradiance, imperfections in the transmission of the optical elements and internal infrared radiation produced by the camera. However, the calibrations conducted by the

FIGURE 2 Infrared transmissivity for the optical components, including the effect of water and CO_2. The bandpass filter (BBP-3670-4020) restricts the recording to 3670-4020 nm, where all transmissions are nearly constant with wavelength.

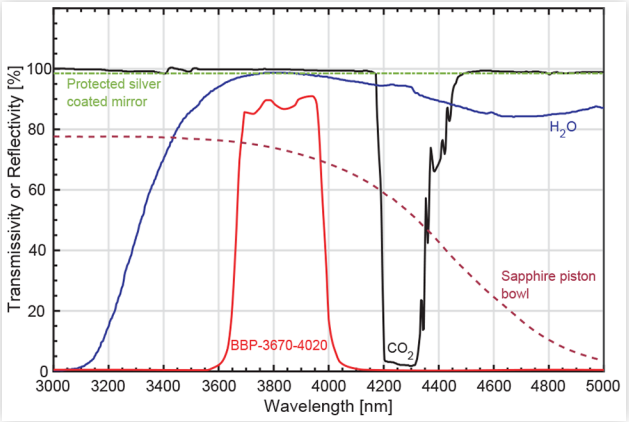

manufacturer are taken under ideal circumstances with a free optical path between the camera lens and a black body (emissivity ≈1). In contrast, this cannot be replicated in the engine due to the transmission and reflectivity losses through the optics required to gain optical access to the combustion chamber which is described in Figures 1 and 2.

The combustion event produces significant amounts of water and CO_2, which are significant absorbers between 3000 and 5000 nm [18]. This absorption can significantly impact the accuracy of computed temperature if it is not accounted for through a custom calibration. Moreover, CO is also a major absorber of radiation within this wavelength however, within the filtered range CO absorption is negligible [19]. In order to mitigate the absorption caused by the CO_2 and water, a bandpass filter (BBP-3670-4020) is employed only to permit radiation between 3670 and 4020 nm, where the transmissivity of water and CO_2 is high, and the flame radiation intensity is low. The permitted band is illustrated in Figure 2. The custom calibration was created using a dummy injector which was designed and fitted to the optical engine. The dummy injector was developed using a Delphi DFI 1.3 nozzle tip and cartridge heater with an aluminium strip going down into the volume usually filled by the needle to provide better heat conduction to the tip. Thermal paste was also used in the

FIGURE 3 Custom calibration generated to compensate for optical transmission losses.

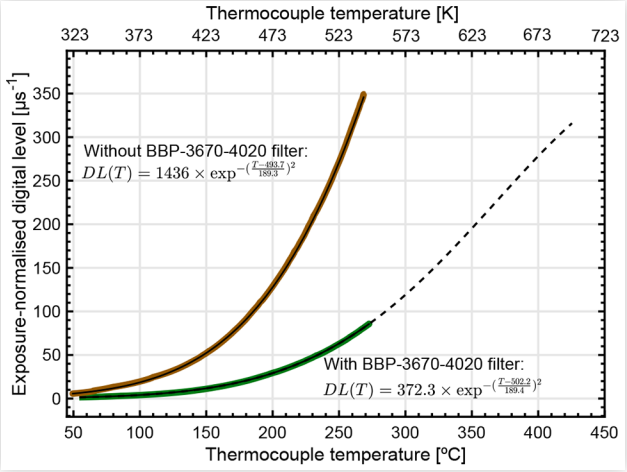

FIGURE 4 Region of interest highlighted as the green area which was applied when processing nozzle temperatures on the incline plane of the DFI 1.3 injector at the location of the nozzle orifices.

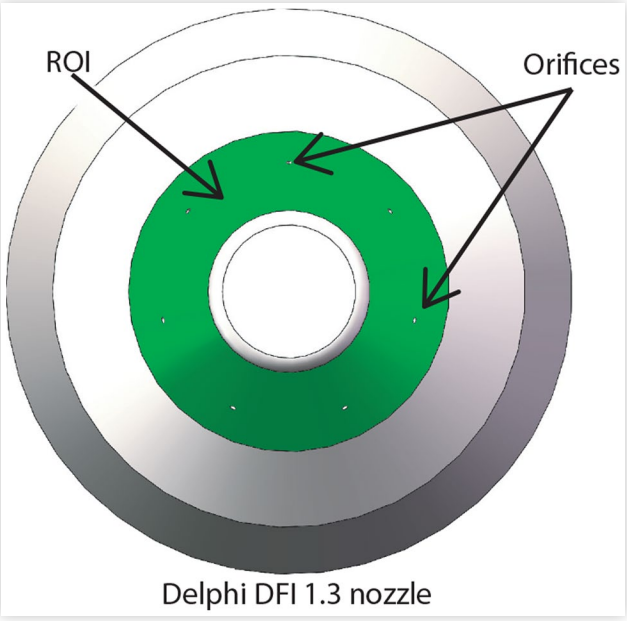

intermediary areas to increase the heat transfer between the cartridge heater and the metallic parts of the injector nozzle. In order to provide feedback to the PID controller and log the temperature of the injector nozzle, thermocouples were fitted into the injector nozzle sac. The dummy injector was then used to emulate the rise in nozzle tip temperature between approximately 50 °C to 270 °C over a period of two hours with the camera recording at 1 fps to capture the change in digital level as the temperature increases (3). To ensure the accuracy of the custom calibration, the infrared camera was allowed to regulate its exposure to maintain optimum pixel well filling. Furthermore, the injector nozzle was coated with soot to increase the emissivity of its surface to ≈0.95 ([20]), compared to that of standard buffed steel finish (emissivity ≈0.16 [21]). However, during engine operation, the infrared camera's automatic exposure control response time is not high enough. Therefore when under engine operating conditions, exposure should be set based on where the interest is. For example, if the interest is peak temperature, the expected peak temperature should meet 60% of the well capacity, which for the Telops camera used is 8 Me-.

To calculate the nozzle temperature from the level of radiation collected by the infrared camera, it first must be understood that the amount of radiation emitted by a surface is a function of its emissivity and temperature, as stated by Kirchoff. Once a high emissivity was obtained by sooting the injector nozzle, data was recorded and processed against the custom calibration discussed previously. The formula for the calibration curve was found and then applied to the digital level values for every pixel of each video frame. Each frame was then cropped to a pre-defined region of interest, shown in Figure 4, and then averaged to get a crank angle based temperature measurement across the cycle (5).

Infrared measurement and Post Processing Methodology

To obtain quantitative results from the raw data collected by the camera's sensor, an algorithm was used as illustrated in Figure 5. The process of converting the raw data collected by the camera's sensor began with normalising for time. As previously discussed, measurements are conducted with different exposure times to prevent over-saturation of the camera sensor; normalising this data for time allows these measurements to be compared irrespective of exposure. Then the data was then cropped to a region of interest (ROI), which is the inclined plane where the injector orifices reside. This ROI is shown in Figure 4. Following the data being cropped to the ROI, the calibration shown in Figure 3 was applied to each individual frame and stored, creating a temperature image stack. Once all the frames had been converted to temperature, the arithmetic mean for each frame is then found. The frame averaged temperature measurements are then stored as a vector to produce a crank-angle resolved temperature trace. Finally, the frame averaged vector stack was then averaged to find the ensemble-averaged temperature, which is then compared against the thermocouple measurements from the instrumented injector to provide a sequence uncertainty. These two data sets are then plotted and validated against the thermocouple. In order to compare the infrared-based temperatures with the instrumented injector, the ensemble-average of the infrared temperature vector was computed to produce the mean nozzle temperature of that video recording, as shown in Figures 5 and 7. Further to the vector plots shown in Figure 7 thermal topology maps were also created to provide a better understanding of the thermal distribution across the nozzle surface under varying operating conditions. Using these four outputs (thermal topological view, frame averaged vector, ensemble-averaged vector and thermocouple measurement), it is possible to gain a much greater insight into the thermal evolution of engine surfaces.

FIGURE 5 Post processing methodology used to obtain an ensemble average of the nozzle tip temperature and frame-averaged temperature to generate a crank-resolved trace.

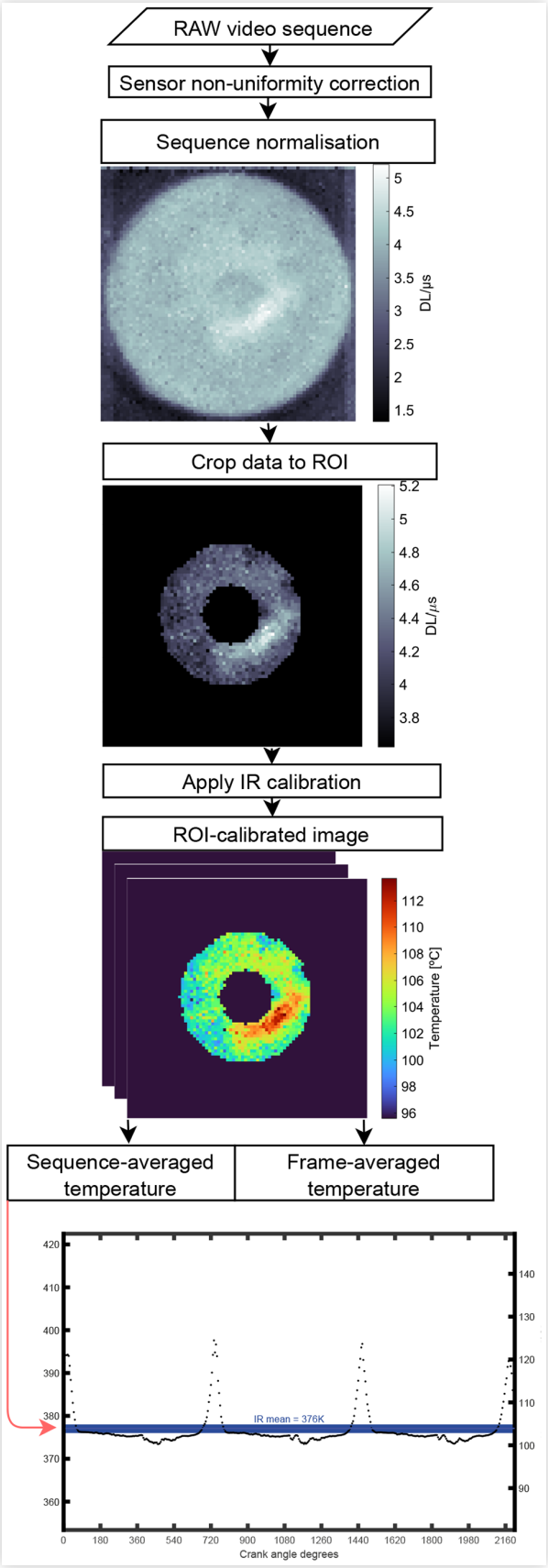

FIGURE 6 Uncertainty analysis of measurements allows the effect of fouling on the optical bowditch piston to be realised. Open black symbols are an ideal case with no engine movement and the optical surfaces clean.

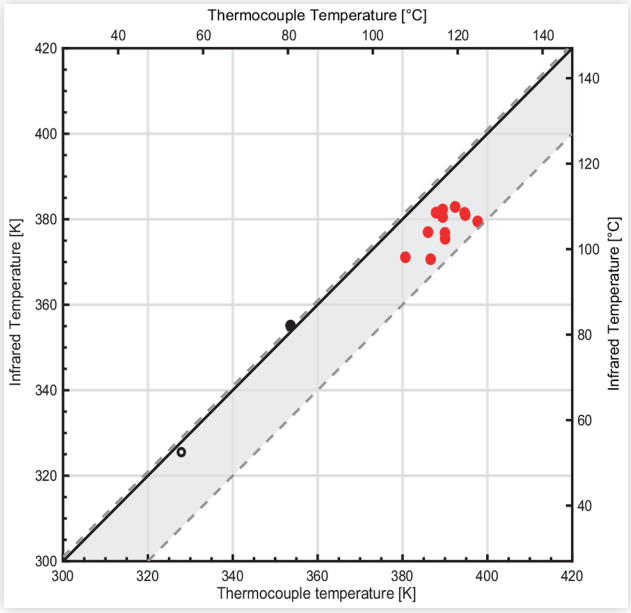

FIGURE 7 Motored case (a) and a fired case (b) to enable the validation of the method by comparing the mean infrared and thermocouple measurements.

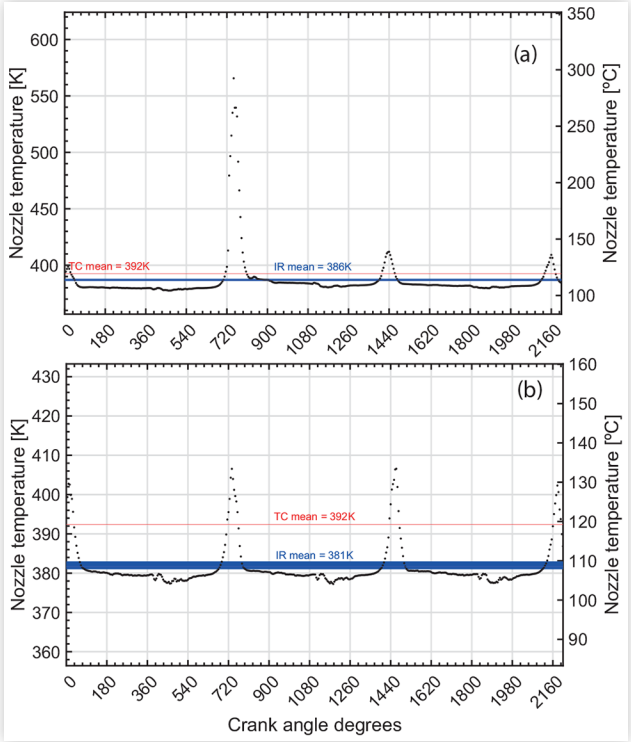

Uncertainty Analysis

An uncertainty analysis was performed to validate the methodology by comparing the thermocouple instrumented injector to the time-averaged infrared video measurements. Figure 6 shows the uncertainty under ideal static conditions (open black dots), fouled static conditions (closed black dots) and motored conditions (red dots). The solid black line marks the ideal error-free measurement. The distribution of the plotted data shows that the thermographic approach consistently under predicts the actual nozzle tip temperature as measured by the thermocouple.

Comparing the measurement under ideal and non-ideal conditions can justify that the thermographic approach consistently yields lower nozzle temperature measurements. The calibration was recorded in an ideal condition when the engine was static with the surfaces of the mirror piston bowl and clean. The clean condition allows for greater transmission of infrared radiation, thus yielding an uncertainty of $^{+20}_{-1}$ K when comparing against the instrumented injector. However, during engine operation under both motored and fired conditions, the optical transmissivity will be reduced by the accumulation of engine by-products which leads to additional absorption in the spectrum of interest. In our measurements, this resulted in uncertainty which never exceeded 20 K.

Additional areas of increased uncertainty are introduced due to low levels of well filling on the camera sensor, which generates an underexposed image leading to an increase in the influence of the sensor's signal to noise ratio on the resultant measurement. However, for this analysis, we can conclude the uncertainty to be estimated as $^{+20}_{-1}$ K.

Figure 7 shows the thermocouple-based compared to the temperatures crank-resolved instantaneous and infrared-based video-averaged temperatures for both motored and fired test conditions. In both cases, the two temperatures agree within 11 K, thus suggesting that the calibration applied and the implementation applied to the infrared thermography are satisfactory.

FIGURE 8 Effect of injection duration on nozzle tip temperature for injections of CEC-RF79 fuel.

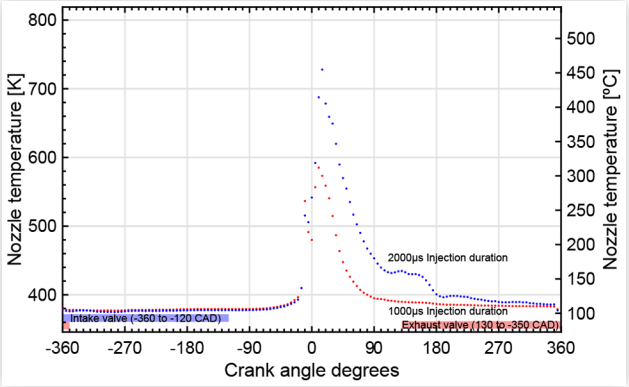

FIGURE 9 Effect of swirl on nozzle tip temperature. Under high swirl conditions the accelerated mixing of the in-cylinder charge leads to cooler and more unstable nozzle tip temperatures during intake cause by a forced convection effect aiding the heat transfer between the gas and the nozzle tip. The same forced convection effect causes higher temperatures during compression and expansion strokes.

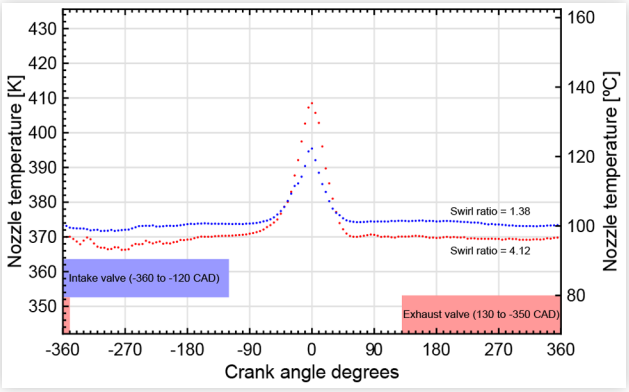

Results

The results below were achieved using the previously discussed methodology and small changes in operating conditions to enable their effect on the injector nozzle tip temperature and homogeneity to be studied. Firstly, Figure 8 shows that longer injection durations lead to an increase in injector nozzle tip temperature due to prolonged exposure to the high-temperature flame and combustion products. Still, during consecutive fired cycles, it would be expected that the thermal floor would rise. The additional heat generated from the cycle is then retained, increasing the peak motored temperature of the next cycle. The increasing thermal floor can be demonstrated in Figure 7b, where the thermal floor between the fired peak and subsequent motored peak is hotter than the thermal floor between the preceding motored peak and the fired peak. If the engine is fired consecutively, the temperature rise would become less abrupt due to cooling caused by the fuel passing through the injector nozzle. The cooling event generated by the fuel injection event is captured in Figure 8 with the temperature rise reverting abruptly towards the end of the compression stroke (-10 to 0° CA aTDC).

After the ignition event, the temperature is retained during the expansion stroke between 0-180° aTDC, as the hot combustion gasses are trapped in the cylinder. However, heat is lost during the expansion stroke towards 180° aTDC, by which point the gas temperature is now cooler than the injector nozzle tip. Due to the gas temperature being cooler than that of the nozzle tip, there is a subsequent cooling effect during the exhaust stroke and the temperature drops close to the thermal floor of the cycle.

Figure 9 shows there is nozzle tip temperature fluctuations during the intake stroke of approximately 5 K. The thermal fluctuations in the intake stroke is generated by inducted gas being significantly cooler than the nozzle tip temperature and the increased forced convection effect due to the increased swirl ratio. Looking further into the cycle, during the compression stroke, the forced convection effect also generates higher peak temperatures due to the increased

FIGURE 10 Increased swirl ratio resulted in a more homogenous temperature distribution across the nozzle surface. The test point was for a motored (non-combusting) cycle.

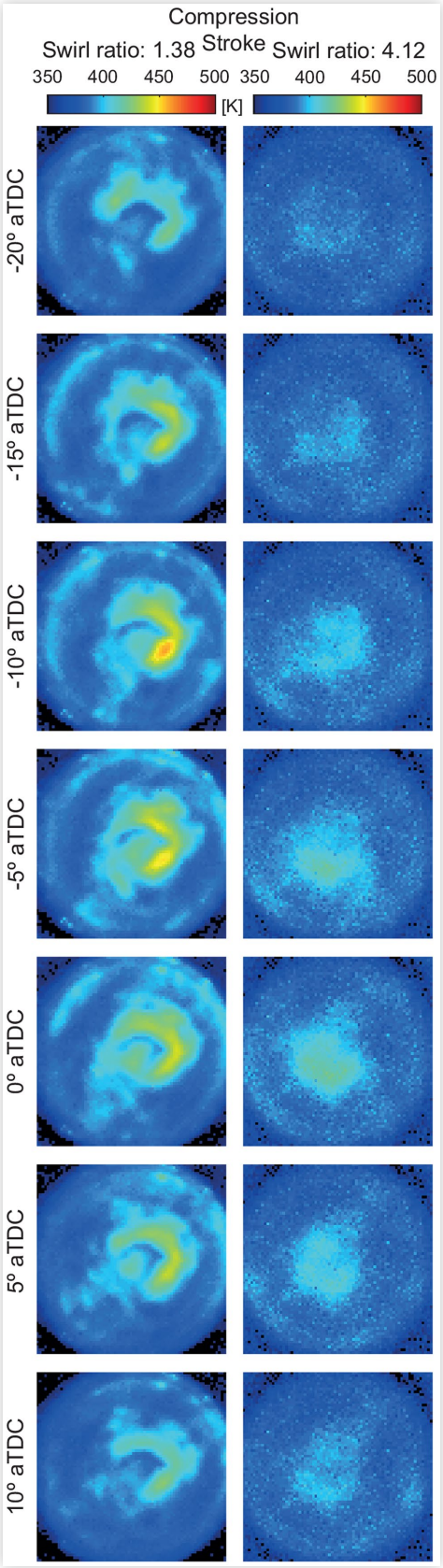

in-cylinder air motion aiding the heat transfer between the hot compressed gas the injector nozzle. Finally, during the expansion and exhaust stroke, the nozzle's thermal stability is high due to the thermodynamic process undertaken earlier in the engine cycle.

However, the homogeneity of the injector nozzle surface generated by the increased swirl does not provide thermal stability of the injector nozzle tip throughout the engine cycle. This effect on the temperature distribution across the nozzle surface is demonstrated by Figure 10 with the test cases being taken with the minimum and maximum swirl ratio of 1.38 and 4.12, respectively. Figure 10 shows that increased swirl leads to a more homogenous nozzle temperature distribution. The more homogenous nozzle temperature is expected to result from the increased air motion leading to more mixing between the hot and cold in-cylinder gases, which in turn leads to a more homogenous temperature across the cylinder and therefore the nozzle tip surface.

Conclusion

This article proposes a method for measuring time-resolved nozzle tip temperature to investigate the effect of varying intensities of in-cylinder air motion and injection duration on injector tip temperature. The measurements demonstrate that increasing the intensity of the in-cylinder swirl yields a more homogenous temperature distribution across the nozzle's surface. Moreover, the increased swirl also generated greater thermal fluctuations during the intake stroke due to the increased turbulent kinetic energy and higher peak temperatures. The investigations also indicated that injection duration could significantly influence the injector nozzle tip temperature over fired conditions.

Acknowledgments

This work was supported by the UK's Engineering and Physical Science Research Council [EPSRC grant EP/S513751/1] and BP International Ltd. Raúl Payri was hosted at the University of Brighton under the Salvador de Madariaga programme [reference PRX18/00243] from Ministerio de Ciencia, Innovacion y universidades from the Spanish Government.

References

1. Zhu, J., Kuti, O.A., and Nishida, K., "Effects of Injection Pressure and Ambient Gas Density on Fuel - Ambient Gas Mixing and Combustion Characteristics of di Diesel Spray," SAE Technical Paper 2011-01-1819 (2011). https://doi.org/10.4271/2011-01-1819.
2. Payri, R., García-Oliver, J.M., Bardi, M., and Manin, J., "Fuel Temperature Influence on Diesel Sprays in Inert and Reacting Conditions," *Applied Thermal Engineering* 35 (2012): 185-195.

3. Hsueh, M.-H. and Lin, D.-F., "The Performance Analysis and Design Optimization of Fuel Temperature Control for the Injection Combustion Engine," *Journal of the Chinese Institute of Engineers* 39, no. 7 (2016): 777-784.
4. Chen, G., "Study of Fuel Temperature Effects on Fuel Injection, Combustion, and Emissions of Direct-Injection Diesel Engines," *Journal of Engineering for Gas Turbines and Power* 131, no. 2 (2008).
5. Rahim, R., Mamat, R., Taib, M.Y., and Abdullah, A.A., "Influence of Fuel Temperature on a Diesel Engine Performance Operating with Biodiesel Blended," *Journal of Mechanical Engineering and Sciences* 2 (2012): 226-236.
6. Payri, R., Salvador, F.J., Carreres, M., and Morena, J.D.L., "Fuel Temperature Influence on the Performance of a Last Generation Common-Rail Diesel Ballistic Injector. Part II: 1d Model Development, Validation and Analysis," *Energy Conversion and Management* 114 (2016).
7. Papadopoulos, N. and Aleiferis, P., "Numerical Modelling of the in-Nozzle Flow of a Diesel Injector with Moving Needle During and After the End of a Full Injection Event," SAE Technical Paper 2015-24-2472 (2015). https://doi.org/10.4271/2015-024-2472.
8. Sykes, D., Turner, J., Stetsyuk, V., de Sercey, G. et al., "Quantitative Characterisations of Spray Deposited Liquid Films and Post-Injection Discharge on Diesel Injectors," *Fuel* 289 (2021): 119833.
9. Sykes, D., Stetsyuk, V., Turner, J., de Sercey, G. et al., "A Phenomenological Model for Near-Nozzle Fluid Processes: Identification and Qualitative Characterisations," *Fuel* 310PA (2022): 122208.
10. Jahangirian, S., Egelja, A., and Li, H., "A Detailed Computational Analysis of Cavitating and Non-Cavitating High Pressure Diesel Injectors," SAE Technical Paper 2016-01-0873 (2016). https://doiorg/10.4271/2016-01-0873.
11. Sykes, D., Sercey, G.D., Gold, M., Pearson, R. et al., "Visual Analyses of End of Injection Liquid Structures and the Behaviour of Nozzle Surface-Bound Fuel in a Direct Injection Diesel Engine," SAE Technical Paper 2019-01-0059 (2019). https://doi.org/10.4271/2019-01-0059.
12. Risberg, P.A., Adlercreutz, L., Aguilera, M.G., Johansson, T. et al., "Development of a Heavy Duty Nozzle Coking Test," SAE Technical Paper 2013-01-2674 (2013). https://doi.org/10.4271/2013-01-2674.
13. Malbec, L.M., Pickett, L.M., Payri, R., Bazyn, T., et al., "Spray A Nozzle Tip Temperature Measurements," in *ECN Workshop*, 2011.
14. Gimeno, J., Martí-Aldaraví, P., Carreres, M., and Peraza, J.E., "Effect of the Nozzle Holder on Injected Fuel Temperature for Experimental Test Rigs and Its Influence on Diesel Sprays," *International Journal of Engine Research* 19, no. 3 (2018): 374-389.
15. Kashdan, J. and Bruneaux, G., "Laser-Induced Phosphorescence Measurements of Combustion Chamber Surface Temperature on a Single-Cylinder Diesel Engine," SAE Technical Paper 2011-01-2049 (2011). https://doi.org/10.4271/2011-01-2049.
16. Stone, C.R. and Ladommatos, N., "The Measurement and Analysis of Swirl in Steady Flow," SAE Technical Paper 921642 (1992). https://doi.org/10.4271/921642.
17. Forte, C., Catellani, C., Cazzoli, G., Bianchi, G.M. et al., "Numerical Evaluation of the Applicability of Steady Test Bench Swirl Ratios to Diesel Engine Dynamic Conditions," *Energy Procedia* 81 (2015): 732-741.
18. Lagueux, P., Tremblay, P., Savary, S., Farley, V. et al., "High-Speed Infrared Imaging for Analysis of a Diesel Engine Supplied with a Premixed Methane-Air Charge," *Measurement Automation Monitoring* 63 (2017).
19. NIST WebBook, "Carbon Monoxide," Accessed on: 17th Dec. 2021. [Online]. Available: https://webbook.nist.gov/cgi/cbook.cgi?ID=C630080Type=IRSPECIndex=1IR-SPEC.
20. De Falco, G., Moggia, G., Sirignano, M., Commodo, M. et al., "Exploring Soot Particle Concentration and Emissivity by Transient Thermocouples Measurements in Laminar Partially Premixed Coflow Flames," *Energies* 10, no. 2 (2017): 232.
21. Gubareff, G.G., *Thermal Radiation Properties Survey: A Review of the Literature* (Honeywell Research Center, 1960)

e-ISSN 2641-9645